ISSN (Print) 1226-1750
ISSN (Online) 2233-6656
Journal of Magnetics 26(2), 146-155 (2021) https://doi.org/10.4283/JMAG.2021.26.2.146

Modeling and Analysis of Magnetized Nanomaterial Williamson Towards a Variable Thicked Surface Subject to Joule Heating and Activation Energy

Wei-Miao Qian[1], Fazal Haq[2]*, M. Ijaz Khan[3], Sohail A. Khan[4], and Shahid Farooq[3]

[1]*School of Continuing Education, Huzhou Vocational & Technical College, Huzhou 313000, P. R. China*
[2]*Department of Mathematical Sciences Karakoram International University Main Campus, Gilgit 15100, Pakistan*
[3]*Department of Mathematics, Riphah International University I-14, Islamabad 44000, Pakistan*
[4]*Department of Mathematics, Quaid-I-Azam University 45320, Islamabad 44000, Pakistan*

(Received 10 March 2021, Received in final form 2 April 2021, Accepted 6 April 2021)

The prime intention of present article is to study the behavior of magnetized Williamson nanofluid. Flow governing model is obtained considering flow over variable thickness surface with convective heat and mass boundary constraints. The effects of Joule heating, Brownian diffusion and thermophoresis are further considered. Moreover, chemical reaction associated with activation energy is accounted. Boundary layer assumptions are used to obtain the dimensional system of differential equations. The system of PDE's are converted into ODE's ones using transformations. Magneto fluids are relatively prevalent in liquid metals, salt water, plasma, metallurgy, cancer therapy and drug delivery target. The considered investigation has relevance in metallurgical processes, polymer industry and plastic sheet. The governing model of ODE's is then tackled via HAM for convergent series solution. Influence of pertinent variables on velocity, concentration, temperature, total entropy rate, skin friction coefficient, Bejan number, local heat and mass transfer rates are studied graphically. Main outcomes are enlisted at the end.

Keywords : variable thickness, activation energy, nonlinear convection, Williamson nanofluid, MHD

1. Introduction

Pseudoplastic fluids frequently occurs in non-Newtonian fluids become a very interesting field of research due to its wide range of applications in manufacturing industries such as coated sheets, suspension photographic films, extrusion of polymer sheets etc. [1]. No doubt the classical Naiver Stokes equations are inadequate to explore the fluid characteristics in rheology. Researchers proposed rheological models to overcome such deficiencies. To explore characteristics of Pseudoplastic fluids a class of models have been suggested such as Ellis model, power law model, Cross model, Carreau model and slight attention has been paid to the Williamson fluid model. Williamson [2] proposed a mathematical model for the flow of pseudoplastic materials and verified the results experimentally. The characteristics of flow in thin layer of Williamson fluid under the influence of gravitational field is studied by Lyubimov and Perminov [3]. Nadeem *et al*. [4] introduced a mathematical model to describe the flow of Williamson material towards stretched surface. Williamson fluid flow near extending surface with Cattanneo-Christov heat flux effects is deliberated by Salahuddin *et al.* [5]. Hayat *et al.* [6] scrutinized magneto-hydrodynamic two dimensional MHD flow of Williamson with melting heat. The effects of thermal radiation and thermo-diffusion in flow of Williamson nanomaterial near a shrinking/stretching porous surface is studied by Bhatti and Rashiddi [7]. Mass and heat transportation in Williamson nanomaterial towards non-uniform slandering sheet with variable thermal properties is reported by Reddy *et al.* [8]. Chemically reactive and radiated flow of Williamson nanomaterial over a linear stretchable horizontal sheet is discussed by Krishnamurthy *et al.* [9]. Peristaltic Williamson nanomaterial flow in a compliant walls channel is examined by Nadeem *et al.* [10].

Effect of magnetic field in electrically conducting materials is known as magnetohydrodynamics (MHD). MHD has vast applications in different fields of engineering and medical sciences like X-ray radiation, solar

©The Korean Magnetics Society. All rights reserved.
*Corresponding author: Tel: +923467505654
Fax: +923467505654, e-mail: fazal.haq@kiu.edu.pk

© 2021 Journal of Magnetics

wind, tumor therapy, plasmas, electrolytes, fusion, star formation, cooling of fission reactors [11-13]. Kothandapani and Prakash discussed convective MHD peristaltic flow of Jeffery nanoliquid [14]. Impact of Newtonian heating and slip conditions on Wlliamson fluid flow over permeable non-uniform stretching sheet is analyzed by Ullah *et al.* [15]. Hayat *et al.* [16] studied MHD flow of incompressible viscous nanofluid with convective boundary conditions over a stretching sheet. MHD flow of nanomaterial with convective mass conditions is presented by Shehzad *et al.* [17]. Khan and Aziz [18] discussed MHD coupled stress incompressible fluid flow over a rotating disk. Heat transfer performance near stagnation point flow of convected Maxwell liquid over a moving vertical porous sheet with thermal radiation effects and induced magnetic field is studied by Ibrahim [17] Few relevant studies are in Res. [18-24].

In modern technology variable thickness has gained extraordinary significance. Surfaces with variable thickness have extensive applications in civil, mechanical and architectural procedures in the fields of engineering and industry. Variable thickness reduces the weight of auxiliary element hence improve the operation of material. However researchers paid a little attention to flows over stretching surfaces having variable thickness [11, 25]. Ramesh *et al.* [26] studied the effects of radiation on stagnation point incompressible flow of Caisson liquid near non isothermal stretching surface with variable thickness. Characteristics of MHD viscous fluid flow over rotating disk with variable thickness and radiation effects is reported by Hayat *et al.* [27]. Zhang *et al.* [28] studied variable thickness tubes having thin-walled square and explored the characteristics which causes bending collapse in cross-section. The MHD stretched tangent flow over a stretching surface is discussed by Hayat *et al.* [29]. Xun *et al.* [30] discussed heat transfer over rotating plate with variable thickness in case of Ostwald-de Waele fluid with decreasing index.

Chemical reaction and activation energy has key role in mass transfer analysis. Chemical reaction has numerous applications in chemical engineering like geothermal reservoirs, recovery of thermal oil, crops damage via freezing, manufacturing of ceramics, cooling of nuclear reactors, food manufacturing production of polymer and dispersion of fog [31, 32]. Some chemical reactions occur very slowly. In order to increase rate of such reactions addition of catalyst plays a vital role. The least energy necessary to initiate a chemical reaction is known as activation energy. Activation energy has numerous applications in the fields of geothermal, oil emulsions and chemical engineering [33-35]. Alshomrani *et al.* [36] discussed the three dimensional flow of chemically reactive Eyring-Powell fluid with heat sink/source and radiation aspects. Khan *et al.* [37] deliberated the impact of chemically reactive flow with nonlinear slip conditions for upper convected Maxwell fluid. Cattaneo-Christove flux is used to study the features of heat and mass transfer. Shafique *et al.* [38] studied the flow of Maxell fluid with heat and mass transport performance over a rotating disk. Combustible mixture flow and irradiative heat flow in a vertical cylinder under force of gravity with activation energy is studied by Bestman [39]. For more recent developments regarding chemical reaction and activation can be referred through [40-46].

Table 1. Numerical results for $f''(0)$, $\theta'(0)$ and $\phi'(0)$, when $\lambda = Ec = Nt = 0.1$, $n_1 = 0.2$, $\beta_t = \beta_c = 0.2$, $\beta_t = \beta_c = 0.2$, $m^* = \Pr = Sc = 1.5$, $E = Nb = 1.0$, $\alpha^* = 0.9$, $\delta = 1.1$.

Order of approximations	$-f''(0)$	$-\theta'(0)$	$-\varphi'(0)$
01	1.16380	0.1539	0.160
05	1.12994	0.1518	0.185
10	1.12660	0.1519	0.199
15	1.12704	0.1519	0.208
20	1.12699	0.1518	0.213
25	1.12700	0.1517	0.217
30	1.12700	0.1516	0.220
35	1.12700	0.1515	0.221
40	1.12700	0.1515	0.222
45	1.12700	0.1515	0.222

Here we investigated the effects of chemical reaction and activation energy on MHD flow of Williamson nanomaterial over a surface with variable thickness in the presence of convective boundary conditions. To the best of our knowledge, Arrhenius activation energy with binary chemical reaction and magnetic field effects with convective boundary conditions in case of nanomaterial Williamson fluid has not been investigated yet. The governing model of ODE's is then tackled via HAM for convergent series solution [47-51]. The comparative study is highlighted in Table 1 and have good agreement.

2. Problem Formulation

Here we considered convective flow of Williamson nanofluid over stretching sheet with non-uniform thickness. Variable thickness of sheet is $y = \delta^*(x+b)^{\frac{1-m^*}{2}}$, note that for $m^* = 1$, thickness of sheet becomes constant. Flow behavior is analyzed in presence of joule heating and activation energy. Furthermore, thermophoresis and Brownian motion effects are also taken consideration in

Table 2. Comparative study of heat transfer rate with Refs. [52, 53].

Pr	Wang [52]	Khan & Pop [53]	Present
0.2	0.1691	0.1691	0.1702
0.7	0.4539	0.4539	0.4538
2.0	0.9114	0.9113	0.9113
7.0	1.8954	1.8954	1.8953
20.0	3.3539	3.3539	3.3539
70.0	6.4622	6.4621	6.4622

energy and concentration expressions. The stretching velocity of sheet is $u_w(x)=a(x+b)^{m^*}$, where a and b are dimensionless constants.

After applying boundary layer assumptions, the governing flow equations are [1-7]:

$$\frac{\partial u}{\partial x}+\frac{\partial u}{\partial y}=0, \tag{1}$$

$$u\frac{\partial u}{\partial x}+v\frac{\partial u}{\partial y}=\nu\frac{\partial^2 u}{\partial y^2}-\sqrt{2}\Gamma\nu\frac{\partial u}{\partial y}\frac{\partial^2 u}{\partial y^2}-\frac{\sigma B_0^2}{\rho_f}u, \tag{2}$$

$$u\frac{\partial T}{\partial x}+v\frac{\partial T}{\partial y}=\alpha\frac{\partial^2 T}{\partial y^2}+\tau\left\{D_B\frac{\partial C}{\partial y}\frac{\partial T}{\partial y}+\frac{D_T}{T_\infty}\left(\frac{\partial T}{\partial y}\right)^2\right\}+\frac{\sigma B_o^2}{(\rho c)_f}u^2, \tag{3}$$

$$u\frac{\partial C}{\partial x}+v\frac{\partial C}{\partial y}=D_B\frac{\partial^2 C}{\partial y^2}+\frac{D_T}{T_\infty}\frac{\partial^2 T}{\partial y^2}-k_r^2(C-C_\infty)\left(\frac{T}{T_\infty}\right)^{n_1}e^{-\frac{E_a}{kT}}, \tag{4}$$

with

$$\left.\begin{aligned} &u=u_w(x)=a(x+b)^{m^*},\quad v=0,\quad -k_f\tfrac{\partial T}{\partial y}=h_1(T_f-T),\\ &-D_f\tfrac{\partial C}{\partial y}=h_2(C_f-C),\quad \text{at } y=\delta^*(x+b)^{\frac{1-m^*}{2}},\\ &u\to 0,\quad T\to T_\infty,\quad C\to C_\infty \text{ as } y\to\infty, \end{aligned}\right\} \tag{5}$$

Here u and v are components of velocity, $u_w(x)$ denotes stretching velocity, Γ Williamson material parameter, α thermal diffusivity, T temperature, ρ_f density of fluid, $\tau=\left(\frac{(\rho c)_p}{(\rho c)_f}\right)$ heat capacity ratio, $(\rho c)_p$ effective heat capacity of nanoparticles, $(\rho c)_f$ heat capacity of nanofluid, c_f convective fluid concentration, B_0 magnetic field strength, D_B Brownian diffusion coefficient, σ electrical conductivity, K_r reaction rate parameter, D_T thermophoresis diffusion coefficient, E_a activation energy, h_1 non-uniform heat transfer co efficient, h_1 non-uniform mass transfer coefficient, T_∞ ambient fluid temperature, ν Kinematic viscosity, k_f thermal conductivity, m^* power index, n_1 fitted rate constant and C_∞ ambient fluid temperature.

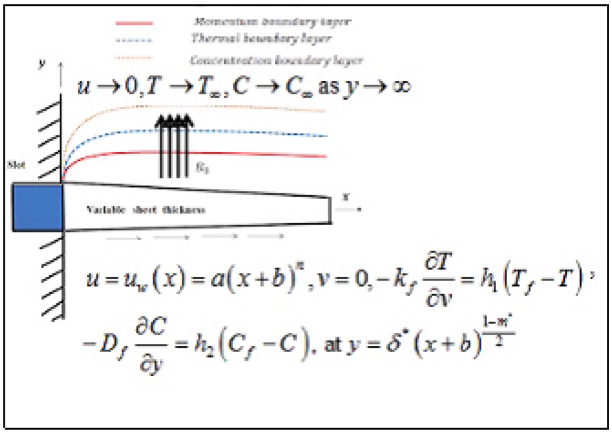

Fig. 1. (Color online) Geometry of the problem.

The transformations are

$$\left.\begin{aligned} &\eta=\sqrt{\left(\tfrac{m^*+1}{2}\right)\tfrac{a}{\upsilon}}(x+b)^{1-m^*}y,\quad \theta=\tfrac{T-T_\infty}{T_f-T_\infty},\quad \phi=\tfrac{C-C_\infty}{C_f-C_\infty},\\ &\Psi=\sqrt{\left(\tfrac{2}{m^*+1}\right)a\nu}(x+b)^{1+m^*},\quad u=a(x+b)^{m^*}F',\\ &v=-\sqrt{\left(\tfrac{m^*+1}{2}\right)\tfrac{a}{\upsilon}}(x+b)^{1-m^*}\left[F+\eta\tfrac{m^*-1}{m^*+1}F'\right], \end{aligned}\right\} \tag{6}$$

Using Eq. (6), Eq. (1) satisfies trivially while equations (2-4) reduce as:

$$F'''+FF''-\frac{2m^*}{m^*+1}F'^2-\lambda F''F'''-\frac{2m^*}{m^*+1}H_a^2F'=0, \tag{7}$$

$$\Theta''+\Pr(F\Theta'+Nb\Theta\Phi+Nt\Theta'^2+EcH_a^2F'^2)=0, \tag{8}$$

$$\Phi''+\frac{N_t}{N_b}\Theta''+ScF\Phi'-\frac{2}{m^*+1}\gamma ScNb\left[1+\delta\Theta\right]^{n_1}\exp\left[\frac{-E}{1+\delta\Theta}\right]\Phi=0, \tag{9}$$

$$\left.\begin{aligned} &F'(\alpha^*)=1, F(\alpha^*)=\alpha^*\left(\tfrac{1-m^*}{1+m^*}\right), \Theta'(\alpha^*)=\beta t\left(1-\Theta(\alpha^*)\right),\\ &\Phi'(\alpha^*)=\beta c\left(1-\Phi(\alpha^*)\right), \text{at } \alpha^*=\delta^*\sqrt{\tfrac{a(m^*+1)}{2\nu}},\\ &F'(\alpha^*)\to 0, \Theta(\alpha^*)\to 0, \Phi(\alpha^*)\to 0, \text{as } \alpha^*\to\infty. \end{aligned}\right\} \tag{10}$$

Where $\alpha^*=\delta^*\sqrt{\frac{a(m^*+1)}{2\nu}}$ is wall thickness parameter.

We define:

$$\left.\begin{aligned} &F(\eta)=f(\eta-\alpha^*)=f(\zeta),\\ &\Theta(\eta)=\theta(\eta-\alpha^*)=\theta(\zeta),\\ &\Phi(\eta)=\phi(\eta-\alpha^*)=\phi(\zeta), \end{aligned}\right\} \tag{11}$$

Eqs. (7-10) takes the form

$$f'''+ff''-\frac{2m^*}{m^*+1}f'^2+\lambda f''f'''-\frac{2m^*}{m^*+1}H_a^2f'=0, \tag{12}$$

$$\theta''+\Pr(f\theta'+Nb\theta\phi+Nt\theta'^2+EcH_a^2f'^2)=0, \tag{13}$$

$$\phi''+\frac{N_t}{N_b}\theta''+Scf\phi'-\frac{2}{m^*+1}\gamma ScNb\left[1+\delta\theta\right]^{n_1}\exp\left[\frac{-E}{1+\delta\theta}\right]\phi=0, \tag{14}$$

$$\left.\begin{aligned} f'(0)=1,\ f(0)=\alpha^*\left(\tfrac{1-m^*}{1+m^*}\right),\ \theta'(\alpha^*)=\beta t\left(1-\theta(\alpha^*)\right),\\ \phi'(\alpha^*)=\beta c\left(1-\phi(\alpha^*)\right),\quad \text{at } \zeta=0,\\ f'(\alpha^*)\to 0,\ \theta(\alpha^*)\to 0,\ \phi(\alpha^*)\to 0,\ \text{as } \zeta\to\infty. \end{aligned}\right\} \tag{15}$$

In above equations H_a^2 denotes Hartman number, λ Weissenberg number, Pr Prandtl number, *Nb* Brownian motion parameter, γ chemical reaction parameter, *Nt* thermophoresis parameter, *Ec* Eckert number, *Sc* Schmidt number, *E* non-dimensional Arrhenius activation energy, β_t thermal Biot number, δ temperature difference parameter and β_c concentration Biot number.

Mathematically:

$$\left.\begin{aligned} H_a^2=\frac{\sigma B_0^2}{a\rho(x+b)^{m^*+1}},\ \lambda=\left(\frac{a^3(x+b)^{3m^*-1}}{\nu}\right)^{\frac{1}{2}},\ \mathrm{Pr}=\frac{\nu}{\alpha},\ Nb=\frac{\tau D_B(C_f-C_\infty)}{\nu},\\ Nt=\frac{\tau D_T}{T_\infty}\frac{(T_f-T_\infty)}{\nu},\ Ec=\frac{u_w^2}{C_f(T_f-T_\infty)},\ Sc=\frac{\nu}{D_B},\ \gamma=\frac{K_r^2}{a}(x+b)^{1-m^*},\\ E=\frac{E_a}{KT_\infty},\ \delta=\frac{T_f-T_\infty}{T_\infty},\ \beta t=\frac{h_1}{K_f\sqrt{\frac{m^*+1}{2}\frac{a}{\nu}(x+b)^{m^*-1}}},\ \beta c=\frac{h_2}{D_f\sqrt{\frac{m^*+1}{2}\frac{a}{\nu}(x+b)^{m^*-1}}}. \end{aligned}\right\} \tag{16}$$

Coefficient of skin friction, Nusselt number and Sherwood number are:

$$\left.\begin{aligned} Cf_x=\frac{2\tau_w}{\rho u_w^2},\\ Nu_x=\frac{x+b}{k_f(T_f-T_\infty)}q_w,\\ Sh_x=\frac{x+b}{D_B(C_f-C_\infty)}q_m, \end{aligned}\right\} \tag{17}$$

Where τ_w denotes surface shear stress, q_w surface heat flux and q_m surface mass flux and are given as:

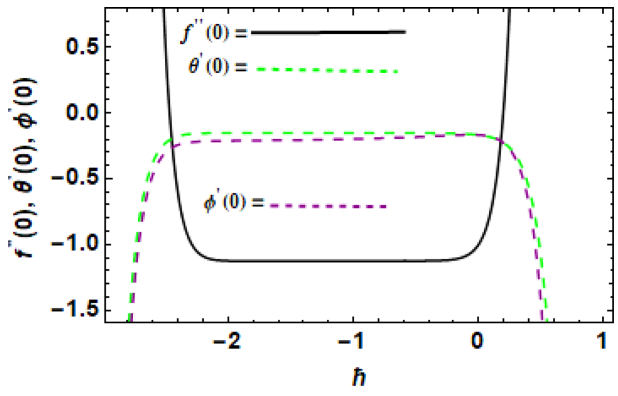

Fig. 2. (Color online) $\hbar-$curves for $f''(0)$, $\theta'(0)$ and $\phi'(0)$.

$$\left.\begin{aligned} \tau_w=\mu\left[\frac{\partial u}{\partial y}-\frac{\Gamma}{2}\left(\frac{\partial u}{\partial y}\right)^2\frac{\partial u}{\partial y}\right]_{y=\delta^*(x+b)^{\frac{1-m^*}{2}}},\\ q_w=-k_f\left(\frac{\partial T}{\partial y}\right)_{y=\delta^*(x+b)^{\frac{1-m^*}{2}}},\\ q_m=-D_B\left(\frac{\partial C}{\partial y}\right)_{y=\delta^*(x+b)^{\frac{1-m^*}{2}}}, \end{aligned}\right\} \tag{18}$$

Using Eq. (18) the non dimensional form of Eq. (17) is

$$\left.\begin{aligned} Cf_x\,\mathrm{Re}_x^{0.5}=\sqrt{\tfrac{m^*+1}{2}}f''(0)+\lambda\tfrac{m^*+1}{4}f'^2(0),\\ Nu_x\,\mathrm{Re}_x^{-0.5}=-\sqrt{\tfrac{m^*+1}{2}}\theta'(0),\\ Sh_x\,\mathrm{Re}_x^{-0.5}=-\sqrt{\tfrac{m^*+1}{2}}\phi'(0). \end{aligned}\right\} \tag{19}$$

Where $\mathrm{Re}_x=\frac{u_w(x)}{\nu}(x+b)$ is local Reynolds number.

3. Series Solution and Convergence Analysis

HAM is use to control the region of convergence in series solution. For this purpose $\hbar$-curves are plotted in Fig. 2. Appropriate values of convergence controlling parameters $\hbar_f$, $\hbar_\theta$ and $\hbar_\phi$ are $-1.8\le\hbar_f\le-0.3$, $-1.7\le\hbar_\theta\le-0.4$ and $-1.4\le\hbar_f\le-0.3$. Suitable initial approximations and linear operators related to the governing equations are taken as follows.

$$\left.\begin{aligned} f_0(\zeta)=1-e^{-\zeta}-\alpha^*\left(\frac{1-m^*}{1+m^*}\right),\\ \theta_0(\zeta)=\frac{\beta_t}{1+\beta_t}e^{-\zeta},\\ \phi_0(\zeta)=\frac{\beta_c}{1+\beta_c}e^{-\zeta}, \end{aligned}\right\} \tag{20}$$

$$\left.\begin{aligned} \pounds_f=f'''-f',\\ \pounds_\theta=\theta''-\theta,\\ \pounds_\phi=\phi''-\phi, \end{aligned}\right\} \tag{21}$$

with

$$\left.\begin{aligned} \pounds_f\left[A_1+A_2e^{\eta}+A_3e^{-\eta}\right],\\ \pounds_\theta\left[A_4e^{\eta}+A_5e^{-\eta}\right],\\ \pounds_\phi\left[A_6e^{\eta}+A_7e^{-\eta}\right], \end{aligned}\right\} \tag{22}$$

where $A_i (i = 1–7)$ are arbitrary constants.

Convergence of equation (12) is obtained in 25th order of approximations, 35 approximations are enough for convergence of Eq. (13) while convergence of Eq. (14) is obtained in 40 iteration.

4. Discussion

The purpose of this section is to analyze the effect of influential parameters on velocity $(f'(\zeta))$, temperature $(\theta(\zeta))$, concentration $(\phi(\zeta))$, skin friction coefficient $(Cf_x \mathrm{Re}_x^{0.5})$, Nusselt number $(Nu_x \mathrm{Re}_x^{-0.5})$ and Sherwood number $(Sh_x \mathrm{Re}_x^{-0.5})$. The values of involved variables taken for plotting graphs are: $\lambda = Ec = 0.1$, $\beta c = 0.2$, $n_1 = 0.5$, $\beta t = Nt = Nb = 0.3$, $E = \mathrm{Pr} = 1.0$, $Ha = 0.8$, $\delta = 1.1$, $m^* = 1.5$, $\gamma = 0.01$, $Sc = 0.7$.

4.1. Velocity field

Figs. 3-6 are drawn to discuss the consequences of thickness parameter (α^*), Hartman number (Ha), Weissenberg number (λ) and power index (m^*) on velocity field $(f'(\xi))$. Fig. 3 portrays the effect of Hartman number on $(f'(\xi))$. It is observed here that $(f'(\xi))$ and thickness of momentum layer decays versus higher Ha. In fact the Lorentz force produces due to magnetic field becomes stronger with the rising Ha, that diminishes the velocity distribution of the nanomaterial. The effect of λ on velocity profile is displayed in Fig. 4. One can observe that the $f'(\xi)$ diminishes versus higher λ. Since λ is ratio of specific process time and relaxation time. Higher

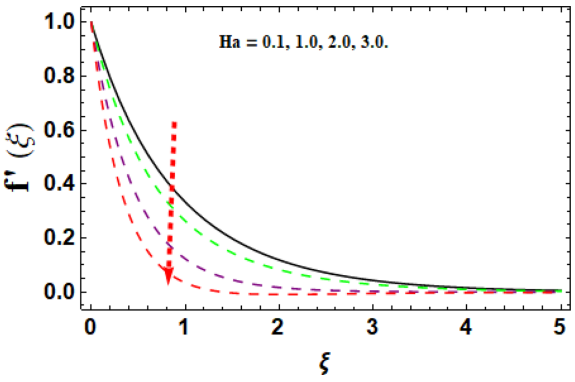

Fig. 3. (Color online) $f'(\zeta)$ versus Ha.

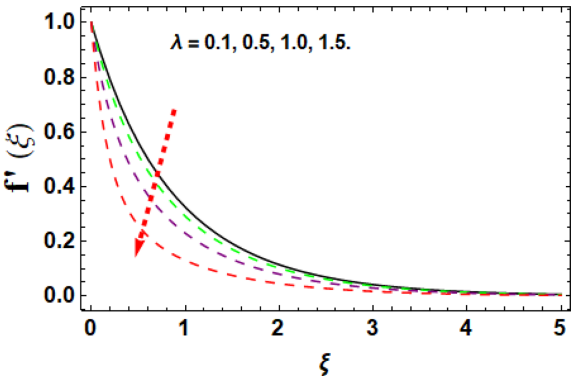

Fig. 4. (Color online) $f'(\zeta)$ versus λ.

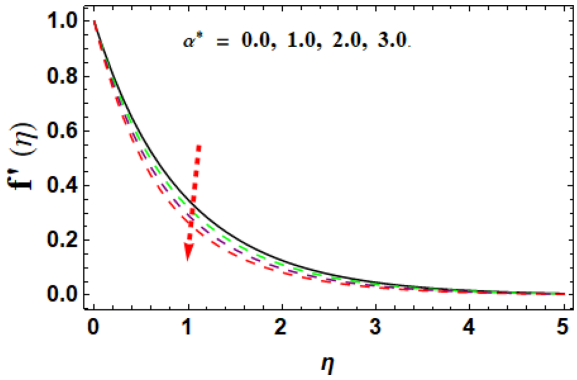

Fig. 5. (Color online) $f'(\zeta)$ versus α^*.

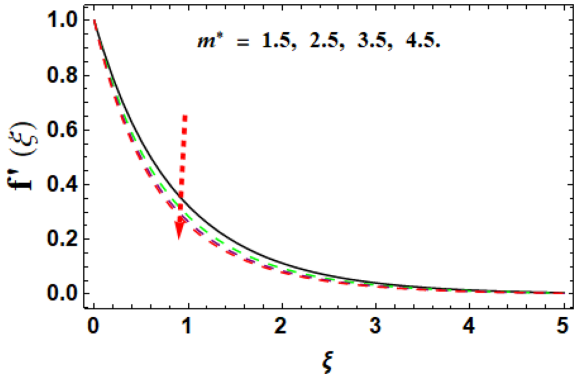

Fig. 6. (Color online) $f'(\zeta)$ versus m^*.

λ enhances the thickness of fluid which causes decay in the velocity and thickness associated layer. Fig. 5 explores the influence of α^* on velocity distribution. Clearly nanofluid velocity and thickness of relevant boundary layer diminishes versus higher α^*. Since when we increase α^* in view of $m^* > 1$, the stretching velocity of sheet boosts consequently nanomaterial velocity and layer thickness diminishes. Characteristics of velocity field versus higher m^* is depicted in Fig. 6, nanomaterial velocity decays in view of higher m^*.

4.2. Temperature field

The effects of Pr, Ec, Ha, Nt, Nb, βt and α^* on temperature field $(\theta(\xi))$ is discussed through Figs. 7-14. Variation in temperature distribution for higher Prandtl number is depicted in Fig. 7. The thermal field and thickness of thermal layer diminishes versus higher Pr. Physically higher Pr improves the thermal diffusivity within liquid. Thus less amount of heat is transferred as a result the $\theta(\xi)$ decays via higher Pr. Fig. 8 is captured to disclose the effect of Ec on thermal field. A decay in temperature profile and thickness of thermal layer is observed versus higher Ec. Effect of Ha on temperature field is depicted in Fig. 9, higher Ha increases temper-

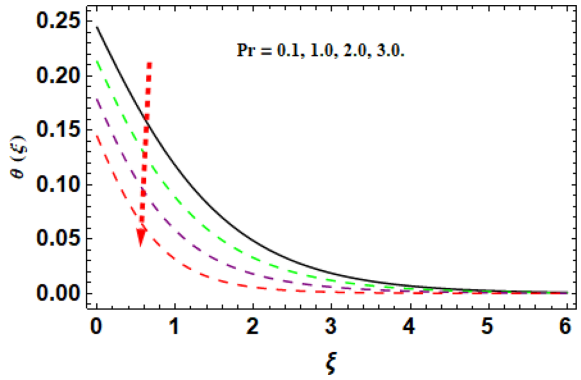

Fig. 7. (Color online) $\theta(\zeta)$ versus Pr.

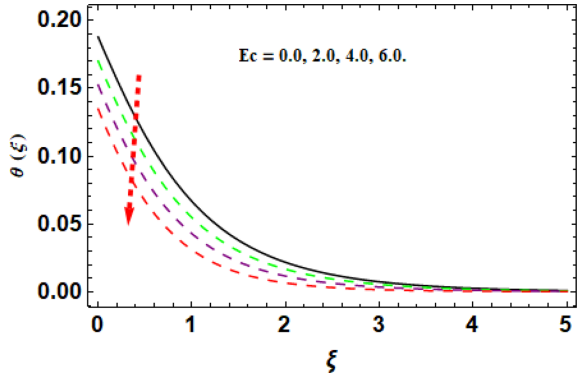

Fig. 8. (Color online) $\theta(\zeta)$ versus *Ec*.

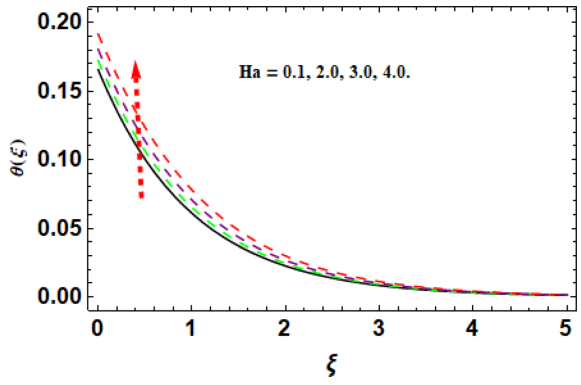

Fig. 9. (Color online) $\theta(\zeta)$ versus *Ha*.

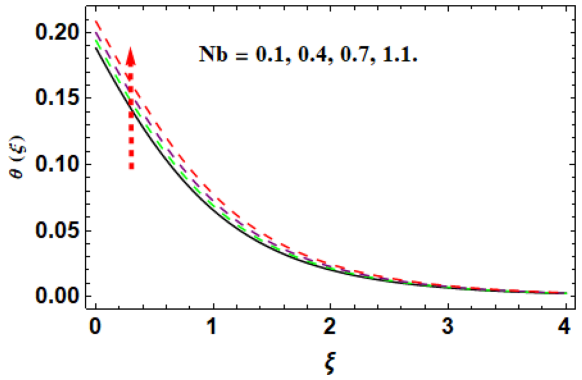

Fig. 10. (Color online) $\theta(\zeta)$ versus *Nb*.

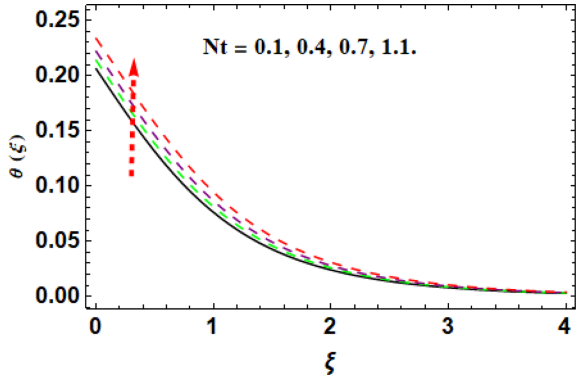

Fig. 11. (Color online) $\theta(\zeta)$ via *Nt*.

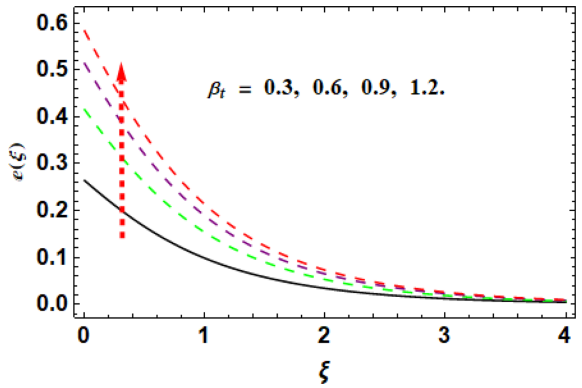

Fig. 12. (Color online) $\theta(\zeta)$ via βt.

ature field and thickness of relevant boundary layer. Since higher *Ha* reduces velocity of nanomaterial as a result thermal field enhances via higher *Ha.* Figs. 10 and 11 elaborates the effects of *Nb* and on temperature profile. It is observed that both *Nt* and *Nb* enhances the thermal field and thickness of related layer. In fact higher *Nb* results an enhancement in random motion of nanoparticles while larger values of *Nt* pulls the fluid particles away from hot surface hence temperature increases in both cases. Variation in temperature distribution due to higher thermal Biot number is depicted in Fig. 12. For higher βt the temperature field and thickness of thermal layer increases. Fig. 13 portrays the effect of wall thickness parameter on temperature profile. The $\theta(\zeta)$ and thermal layer thickness are decreasing functions of α^*. Physically when α^* increases velocity of fluid decreases hence less amount of heat is transfer from sheet to the fluid. Consequently the thermal field diminishes in view of higher α^*. The behavior of temperature field versus higher m^* is captured in Fig. 14. Clearly thermal field and thickness of associated layer decays versus higher m^*.

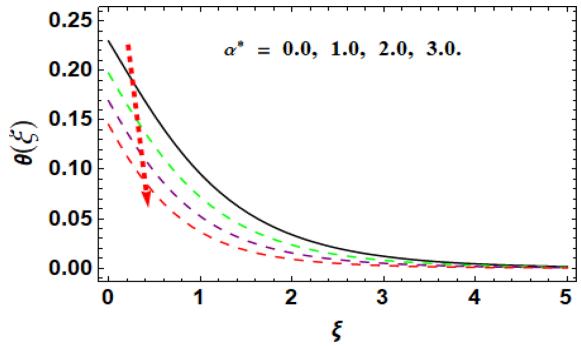

Fig. 13. (Color online) $\theta(\zeta)$ via α^*.

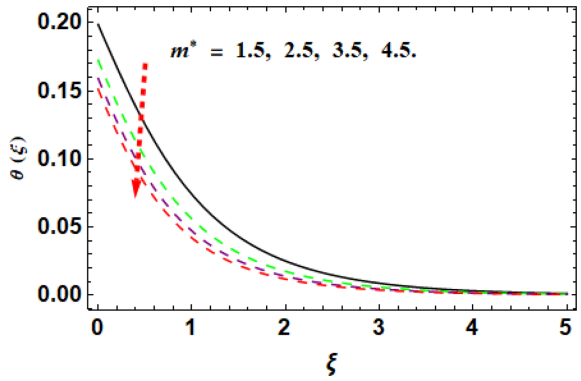

Fig. 14. (Color online) $\theta(\zeta)$ via m^*.

4.3. Concentration

The effect of α^*, δ, γ, E, βc, Nt, Nb and Sc on concentration distribution ($\phi(\xi)$) is discussed through Figs. 15-21. Fig. 15 is plotted to discuss the effect of α^* on mass concentration field. It can be observed that the $\phi(\xi)$ and thickness of concentration layer diminishes for higher α^*. The influence of δ on nanomaterial mass concentration is captured in Fig. 16, improvement in $\phi(\xi)$ and thickness of relevant boundary layer is observed via higher δ. Fig. 17 explores the effect of activation energy (E) on mass concentration. One can observe from Fig. 17 that mass concentration of nanomaterial upshots for higher E. Since, lower temperature and higher activation energy causes low reaction rate, which reduces the rate of chemical reaction as a result mass concentration increases. Fig. 18 elucidates the effect of γ on concentration field. An increment in $\phi(\xi)$ and layer thickness is observed versus higher γ. Effect of Sc on $\phi(\zeta)$ is depicted in Fig. 19. For higher Sc decay in concentration field is noticed.

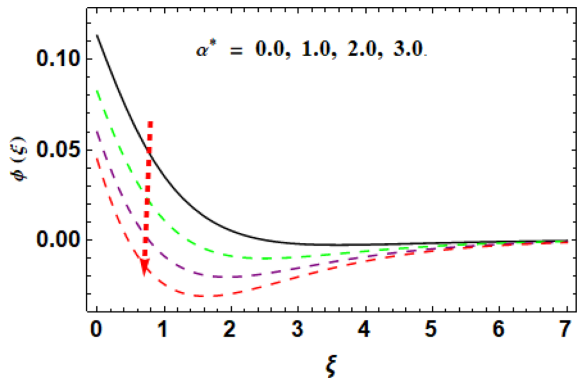

Fig. 15. (Color online) $\phi(\zeta)$ via α^*.

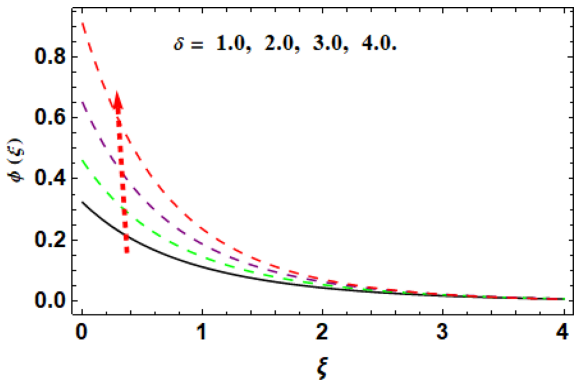

Fig. 16. (Color online) $\phi(\zeta)$ via δ.

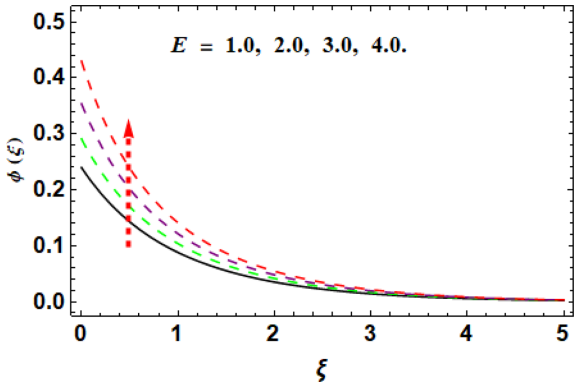

Fig. 17. (Color online) $\phi(\zeta)$ via E.

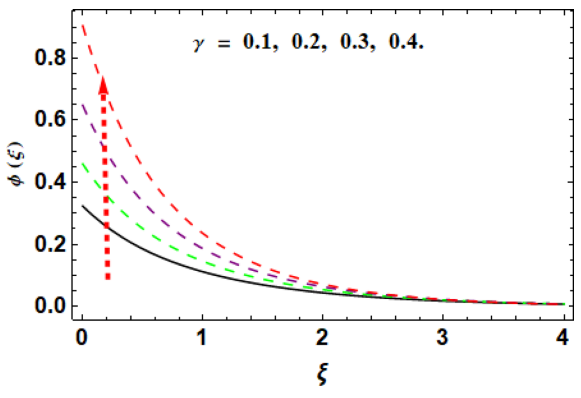

Fig. 18. (Color online) $\phi(\zeta)$ via γ.

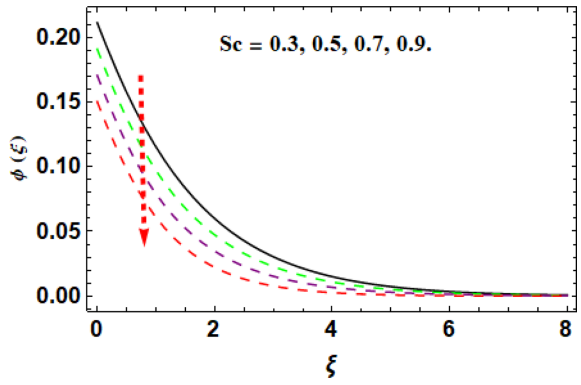

Fig. 19. (Color online) $\phi(\zeta)$ via *Sc*.

4.4. Skin friction, Nusselt and Sherwood numbers

In this subsection, we discuss the impact of pertinent variables on surface drag force (Skin friction coefficient), heat transfer rate (Nusselt number) and mass transfer rate (Sherwood number). The combined effect of Hartman number (*Ha*) and wall thickness parameter (α^*) on surface drag force $(Cf_x \mathrm{Re}_x^{0.5})$ is sketched in Fig. 20. Magnitude of $(Cf_x \mathrm{Re}_x^{0.5})$ upsurges versus higher *Ha* and α^*. Impact of power index (m^*) and Weissenberg number (λ) on $(Cf_x \mathrm{Re}_x^{0.5})$ is depicted in Fig. 21. Here we observe that

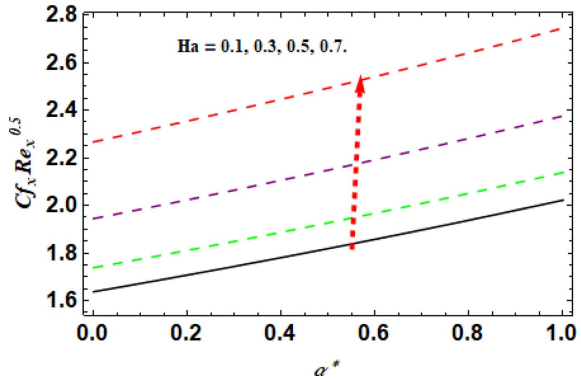

Fig. 20. (Color online) Effect of *Ha* and α^* on $Cf_x \mathrm{Re}_x^{0.5}$.

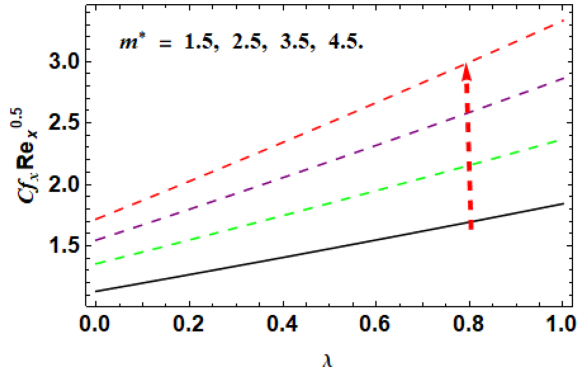

Fig. 21. (Color online) Effect of λ and m^* on $Cf_x \mathrm{Re}_x^{0.5}$.

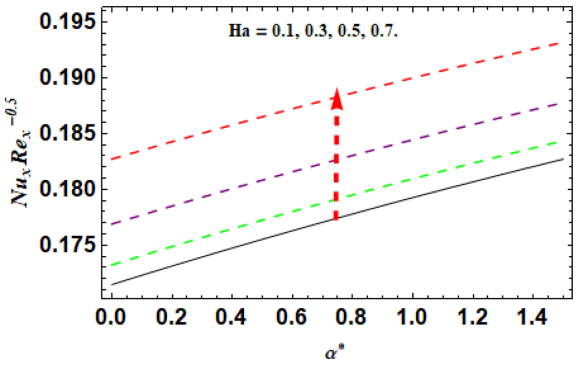

Fig. 22. (Color online) Effect of *Ha* and α^* on $Nu_x \mathrm{Re}_x^{-0.5}$.

$(Cf_x \mathrm{Re}_x^{0.5})$ monotonically increases versus higher m^* and λ. Fig. 22 is sketched to discuss the characteristics of heat transfer rate versus rising values of α^* and *Ha*. Magnitude of Nusselt number is increasing function of α^* and *Ha*. Effect of Pr and *Ha* on Nusselt number is captured in Fig. 23. From Fig. 23 one can observe that Nusselt number increases monotonically for rising Pr and fixed values of *Ha*. Impact of α^* and activation energy parameter (*E*) on mass transfer rate is depicted in Fig. 24. Magnitude of Sherwood number decays for higher α^* and *E*. Fig. 25 is delineated to discuss the behavior of Sherwood number against higher Schmidt number (*Sc*) and reaction rate

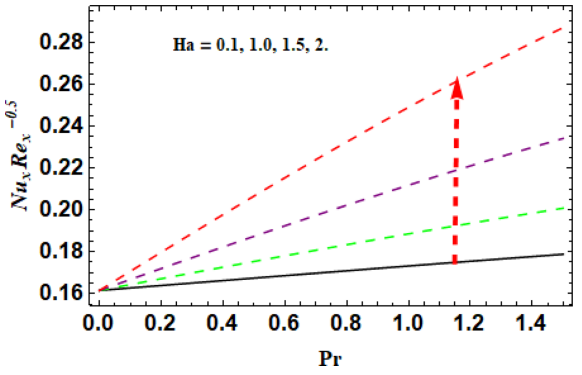

Fig. 23. (Color online) Effect of *Ha* and Pr on $Nu_x \mathrm{Re}_x^{-0.5}$.

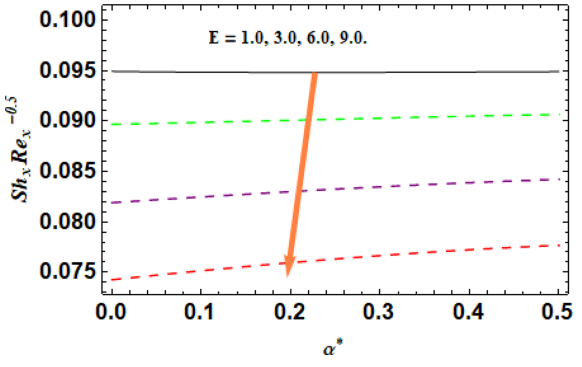

Fig. 24. (Color online) Effect of *E* and α^* on $Sh_x \mathrm{Re}_x^{-0.5}$.

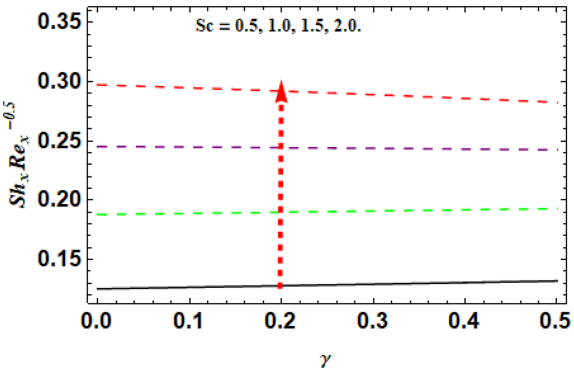

Fig. 25. (Color online) Effect of Sc and γ on $Sh_x \, \mathrm{Re}_x^{-0.5}$.

parameter (γ), clearly magnitude of mass transfer increases for rising Sc and γ.

5. Conclusions

The main observations are:

- Reverse impact of Hartman number is noted for velocity and temperature of nanofluid.
- Velocity, temperature and mass concentration decays versus rising wall thickness parameter.
- Temperature of nanomaterial enhances against Brownian movement and thermophoresis parameter.
- Magnitude of skin friction enhances for higher values of wall thickness parameter and Hartman number.
- Intensity of Nusselt number increases versus higher Prandtl number and Hartman number.
- Magnitude of mass concentration reduces versus Schmidt number and activation energy parameter.

References

[1] E. Felder and C. Levrau, Tribology International **44**, 845 (2011).
[2] R. V. Williamson, Industrial & Engineering Chemistry **21**, 1108 (1929).
[3] V. Lyubimov and D. Perminov, Journal of Engineering Physics and Thermophysics **75**, 920 (2002).
[4] P. D. S. Nadeem, S. Hussain, and C. Lee, Brazilian Journal of Chemical Engineering **30**, 619 (2013).
[5] T. Salahuddin, M. Y. Malik, A. Hussain, S. Bilal, and M. Awais, Journal of Magnetism and Magnetic Materials **401**, 991 (2016).
[6] T. Hayat, G. Bashir, M. Waqas, and A. Alsaedi, Journal of Molecular Liquids **223**, 836 (2016).
[7] M. M. Bhatti and M. M. Rashidi, Journal of Molecular Liquids **221**, 567 (2016).
[8] C. S. Reddy, K. Naikoti, and M. M. Rashidi, Transactions of A Razmadze Mathematical Institute **171**, 195 (2017).
[9] M. R. Krishnamurthy, B. C. Prasannakumara, B. J. Gireesha, and R. S. R. Gorla, Engineering Science and Technology, an International Journal **19**, 53 (2016).
[10] S. Nadeem, E. N. Maraj, and N. S. Akbar, Applied Nanoscience **4**, 511 (2014).
[11] S. Qayyum, T. Hayat, S. A. Shehzad, and A. Alsaedi, Nuclear Engineering and Technology **49**, 1636 (2017).
[12] T. Hayat, A. Shafiq, and A. Alsaedi, Alexandria Engineering Journal **55**, 2229 (2016).
[13] T. Hayat, S. Bibi, M. Rafiq, A. Alsaedi, and F. M. Abbasi, Journal of Magnetism and Magnetic Materials **401**, 733 (2016).
[14] M. Kothandapani and J. Prakash, Applied Nanoscience **6**, 323 (2016).
[15] I. Ullah, S. Shafie, and I. Khan, Journal of King Saud University Science **29**, 250 (2017).
[16] S. A. Shehzad, T. Hayat, and A. Alsaedi, Bulletin of the Polish Academy of Sciences Technical Sciences **63**, 465 (2015).
[17] W. Ibrahim, Propulsion and Power Research **5**, 164 (2016).
[18] S. A. Khan, T. Hayat, A. Alsaedi, and B. Ahmad, Renewable and Sustainable Energy Reviews **140**, 110739 (2021).
[19] K. L. Hsiao, Applied Thermal Engineering **112**, 1281 (2017).
[20] M. Turkyilmazoglu, ACM Transactions on Modeling and Computer Simulation **27**, 3106373 (2017).
[21] M. Turkyilmazoglu, Applied Mathematical Modelling **71**, 1 (2019).
[22] K. L. Hsiao, International Journal of Heat and Mass Transfer **112**, 983 (2017).
[23] K. L. Hsiao, Applied Thermal Engineering **98**, 850 (2016).
[24] M. I. Khan, International Communications in Heat and Mass Transfer **122**, 105177 (2021).
[25] M. Waqas, M. Farooq, M. I. Khan, A. Alsaedi, T. Hayat, and T. Yasmeen, International Journal of Heat and Mass Transfer **102**, 766 (2016).
[26] G. K. R. Prasanna, B. C. Kumara, B. Gireesha, and M. M. Rashidi, Journal of Applied Fluid Mechanics **9**, 1115 (2016).
[27] T. Hayat, S. Qayyum, M. Imtiaz, and A. Alsaedi, Results in Physics **7**, 156 (2017).
[28] X. Zhang, H. Zhang, and Z. Wang, International Journal of Mechanical Sciences **106**, 107 (2016).
[29] T. Hayat, M. Waqas, A. Alsaedi, G. Bashir, and F. Alzahrani, Journal of Molecular Liquids **229**, 178 (2017).
[30] S. Xun, J. Zhao, L. Zheng, X. Chen, and X. Zhang, International Journal of Heat and Mass Transfer **103**, 1214 (2016).
[31] T. Hayat, S. Ahmad, M. I. Khan, and A. Alsaedi, Physica B: Condensed Matter **537**, 116 (2018).
[32] T. Hayat, S. Ahmad, M. I. Khan, and A. Alsaedi, Results in Physics **8**, 545 (2018).
[33] M. I. Khan, T. Hayat, M. I. Khan, and A. Alsaedi, International Communications in Heat and Mass Transfer **91**, 216 (2018).
[34] R. K. Kumar, G. V. Kumar, C. S. K. Raju, S. A. Shehzad,

and S. V. K. Varma, Journal of Physics Communications **2**, 035004 (2018).
[35] K.-L. Hsiao, Energy **130**, 486 (2017).
[36] A. S. Alshomrani, M. Z. Ullah, S. S. Capizzano, W. A. Khan, and M. Khan, Arabian Journal for Science and Engineering **44**, 579 (2018).
[37] M. I. Khan, M. Waqas, T. Hayat, M. I. Khan, and A. Alsaedi, Journal of the Brazilian Society of Mechanical Sciences and Engineering **39**, 4571 (2017).
[38] Z. Shafique, M. Mustafa, and A. Mushtaq, Results in Physics **6**, 627 (2016).
[39] A. R. Bestman, International Journal of Energy Research **15**, 179 (1991).
[40] S. Qayyum, T. Hayat, A. Alsaedi, and B. Ahmad, International Journal of Mechanical Sciences **134**, 306 (2017).
[41] B. Ali, P. K. Pattnaik, R. A. Naqvi, H. Waqas, and S. Hussain, Thermal Science and Engineering Progress 100863 (2021).
[42] M. Azam, F. Mabood, T. Xu, M. Waly, and I. Tlili, Results in Physics **19**, 103576 (2020).
[43] M. Irfan, K. Rafiq, M. Khan, M. Waqas, and M. S. Anwar, International Communications in Heat and Mass Transfer **120**, 105051 (2021).
[44] P. Yang, C. Liu, Q. Guo, and Y. Liu, Journal of Materials Science & Technology **72**, 162 (2021).
[45] B. Ali, P. K. Pattnaik, R. A. Naqvi, H. Waqas, and S. Hussain, Thermal Science and Engineering Progress 100863 (2021).
[46] M. Ramzan, H. Gul, S. Kadry, and Y.-M. Chu, International Communications in Heat and Mass Transfer **120**, 104994 (2021).
[47] S. J. Liao, Springer, Heidelberg, Germany (2012).
[48] S. Han, L. Zheng, C. Li, and X. Zhang, Applied Mathematics Letter **38**, 87 (2014).
[49] M. Turkyilmazoglu, Physics of Fluids **21**, 106104 (2009).
[50] M. Turkyilmazoglu, International Journal of Thermal Sciences **50**, 88 (2011).
[51] M. Turkyilmazoglu, Journal of Applied Mechanics **78**, 021005 (2011).
[52] C. Y. Wang, Applied Mathematics and Mechanics **69**, 418 (1989).
[53] W. A. Khan and I. Pop, International Journal of Heat and Mass Transfer **53**, 2477 (2010).